

Bearings-Only TMA from Electromagnetic and Acoustic Waves

Nabil Amirach, Claude Jauffret, Annie-Claude Perez, Dann Laneuville

▶ **To cite this version:**

Nabil Amirach, Claude Jauffret, Annie-Claude Perez, Dann Laneuville. Bearings-Only TMA from Electromagnetic and Acoustic Waves. 19th International Conference on Information Fusion (FUSION), Jul 2016, heidelberg, Germany. pp.1901-1908. hal-03661352

HAL Id: hal-03661352

https://univ-tln.hal.science/hal-03661352

Submitted on 6 May 2022

HAL is a multi-disciplinary open access archive for the deposit and dissemination of scientific research documents, whether they are published or not. The documents may come from teaching and research institutions in France or abroad, or from public or private research centers.

L'archive ouverte pluridisciplinaire **HAL**, est destinée au dépôt et à la diffusion de documents scientifiques de niveau recherche, publiés ou non, émanant des établissements d'enseignement et de recherche français ou étrangers, des laboratoires publics ou privés.

Bearings-Only TMA from Electromagnetic and Acoustic Waves

Nabil Amirach, Claude Jauffret, Annie-Claude Pérez
Université de Toulon
IM2NP, UMR 7334
83957 La Garde, France
{amirach, jauffret, annie-claude.perez}@univ-tln.fr

Dann Laneuville
DCNS-RESEARCH/CEMIS
44340 Bouguenais, France
dann.laneuville@dcnsgroup.com

***Abstract*—This paper presents a novel BOTMA based upon two types of bearing measurements: the angles of arrival of electromagnetic waves and the angles of arrival of acoustic waves. The difference of the propagation delays makes the problem observable even when the observer is motionless or non-maneuvering. We construct a recursive estimator (using the extended Kalman filter) and a batch estimator (the maximum likelihood estimator) whose respective performances are evaluated by Monte-Carlo simulations, and compared to the Cramér-Rao lower bound.**

Keywords— Bearings-only TMA, Cramér-Rao lower bound, estimation, extended Kalman filter, Fisher information matrix, maximum likelihood estimator, observability.

I. INTRODUCTION

The conventional bearings-only target motion analysis (BOTMA) has been widely addressed in the literature [1-4]. The target is assumed to be in constant velocity (CV) motion. A well-known weakness of it is the need for the platform to maneuver to render the problem observable [5-7]. But, maneuvering makes the observer indiscreet, which is awkward in underwater warfare. This is why constructing target motion analyses (TMA) which need no observer's maneuver to insure observability of the target's trajectory is of prime interest. A few solutions were proposed in the literature: for example, exploiting Doppler-shifted frequency measurement together with bearings makes the problem observable [8-10]. But bearings and frequencies TMA imposes a narrow band processing in the sonar systems. In some circumstances, a target performing particular maneuvers is observable in BOTMA [11-13], from a nonmaneuvering platform.

Another promising way is to exploit the angles of arrival of two kinds of signals propagating with different speeds, such as the angles of "lines of sight" (in other words, electromagnetic waves – EMW -) assumed to instantaneously propagate and the angles of "lines of sound" (or acoustic waves – AW-) whose propagation speed is much lower. A novel TMA using these angle measurements acquired by a unique platform allows passively estimating the trajectory of a target in CV motion without any maneuver of the observer. The bearings of the EMW and the bearings of the AW are named subsequently instantaneous bearings and delayed bearings.

In FUSION'15, two independent papers addressed the problem of instantaneous-bearings-and-delayed-bearings-TMA, called in [15] inverse triangulation TMA (ITTMA) by two different ways: In [14], the authors construct a recursive estimate using an Unscented Kalman Filter (UKF) for BOTMA (whose input is the instantaneous bearings), coupled with an Unscented Gauss-Helmert Filter (UGHF) whose role is to update the current estimate by the delayed bearings (called out of sequence measurements in [14] and [23]). The recursive estimation is done by the two filters: UKF with a 4-dimensional state vector and UGHF with a 5-dimensional state vector. In [15], observability of the target's trajectory is proven and the maximum likelihood estimate is proposed.

In this study, we propose to exploit the analytic link between the propagation delay of the AW and the state vector defining the target's trajectory. This allows us to use one filter (actually an extended Kalman filter – EKF -) with one sole 4-dimensional state vector. We compute also the maximum likelihood estimator (MLE) by the Gauss-Newton routine. The respective empirical covariance matrices (evaluated by Monte-Carlo simulations) of the recursive and batch estimators are compared to the Cramér-Rao lower bound (CRLB).

Taking propagation delay into account was previously addressed: In [16-22], the time delay is on-line estimated to reduce the bias of the estimator of targets position. Most of the time, this time delay appears as a "drawback" of the propagation phenomena. In this paper, it helps to propose a "low-cost" unbiased estimation of the target trajectory.

Our paper is composed of four main sections:

Section II is devoted to the definition of our problem. We give the notations employed subsequently.

In Section III, we give the asymptotic performance of any unbiased estimator through the Cramér-Rao lower bound expression.

The estimations of the trajectory, by the maximum likelihood method, then by the extended Kalman filter, are presented in section IV.

Section V is devoted to Monte-Carlo simulations, which allows us to compare the respective performance of the batch and the recursive estimation.

A conclusion follows.

II. Problem Statement and Notation

Consider a target (T) moving with a constant velocity (or CV motion) and a passive observer (O). In a Cartesian coordinate system, the position of the target at time t is denoted $P_T(t) = [x_T(t) \quad y_T(t)]^T$ and its velocity is $V_T = [\dot{x}_T \quad \dot{y}_T]^T$. The trajectory of the target obeys the following equation: $P_T(t) = P_T(t^*) + (t - t^*)V_T$, t^* being an arbitrary reference time, and is entirely characterized by the chosen state vector $X(t^*) = [x_T(t^*) \quad y_T(t^*) \quad \dot{x}_T \quad \dot{y}_T]^T$. The location of the observer at time t is denoted $P_O(t) = [x_O(t) \quad y_O(t)]^T$. The position of the target relatively to the observer is defined as $P_{OT}(t) = P_T(t) - P_O(t) = r(t)[\sin\theta(t) \quad \cos\theta(t)]^T$. During the scenario, the target and the observer are never located at the same place, *i.e.* $P_{OT}(t) \neq [0 \quad 0]^T$, $\forall\, t$ (see Fig. 1).

The target and the observer are moving in a medium in which the electromagnetic waves (EMW) and the acoustic waves (AW) propagate. Delayed bearings are collected by a passive sonar, whose sampling period is about few seconds (typically 4 seconds), and instantaneous bearings are acquired by a passive radar (the sampling period is 1 second) or an optical device, for example a periscope (it is reasonable to assume that a bearing is measured every 2 minutes), for a submarine at surface.

The propagation delay of the EMW is negligible, whereas that of the AW must be taken into consideration. So, from the viewpoint of the observer, the instantaneous bearing is equal to $\theta(t) = \tan^{-1}\left(\frac{x_T(t)-x_O(t)}{y_T(t)-y_O(t)}\right)$ and the delayed bearing is $\theta_D(t) = \tan^{-1}\left(\frac{x_T(t-\tau(t))-x_O(t)}{y_T(t-\tau(t))-y_O(t)}\right)$, where $\tau(t)$ is the propagation duration of the AW to reach the observer at time t. In other words, the observer detects at time t an AW emitted by the target at time $t - \tau(t)$. Hence, the propagation delay $\tau(t)$ satisfies the recursion $\tau(t) = \frac{\|P_T(t-\tau(t)) - P_O(t)\|}{c}$, where c is the propagation speed of sound in the medium. It can be computed by the following expression,

$$\tau(t) = \frac{\sqrt{[V_T^T P_{OT}(t)]^2 + (c^2 - \|V_T\|^2)\|P_{OT}(t)\|^2} - V_T^T P_{OT}(t)}{(c^2 - \|V_T\|^2)}.$$

Note that this expression is the generalized version of $\tau(t)$ given in [15].

In order to emphasize the fact that $\theta(t)$ and $\theta_D(t)$ are completely defined by the state vector, we will denote them by $\theta(X(t^*), t)$ and $\theta_D(X(t^*), t)$, respectively.

At time u_k (respectively v_k), the observer acquires the measured angles $\theta_m(u_k)$, respectively $\theta_{D,m}(v_k)$, defined by $\theta_m(u_k) = \theta(u_k) + \varepsilon(u_k)$ and $\theta_{D,m}(v_k) = \theta_D(v_k) + \varepsilon_D(v_k)$.

$\varepsilon(u_k)$ and $\varepsilon_D(v_k)$ are the additive noises, assumed to be zero-mean and Gaussian. Their covariance matrices are respectively equal to $diag(\sigma^2)$ and $diag(\sigma_D^2)$ (assumed to be known). Note that, in this paper, the delayed bearings are assumed to be unbiased.

We aim to estimate the trajectory of the target from the two sets $\{\theta_m(u_k),\ k = 1, 2, \dots, N\}$ and $\{\theta_{D,m}(v_k),\ k = 1, 2, \dots, N_D\}$.

In order to simplify the coming developments, we define the three following sets: $\mathcal{U} \triangleq \{u_k,\ k = 1, 2, \dots, N\}$ is the set of the acquisition time of instantaneous bearings; $\mathcal{V} \triangleq \{v_k,\ k = 1, 2, \dots, N_D\}$ is the set of the acquisition time of delayed bearings; and $\mathcal{T} \triangleq \mathcal{U} \cup \mathcal{V}$. We sort the elements of $\mathcal{T}$ in the chronological order: $\mathcal{T} = \{t_1, t_2, \dots, t_M\}$, with $t_k < t_{k+1}$. Then we define two subsets of $\{1, 2, \dots, M\}$ denoted I (as "instantaneous") and D (as "delayed") as follows: $k \in I$ if the observer acquires a EMW angle at time t_k; $k \in D$ if the observer acquires a AW angle at time t_k.

Now, our problem can be rephrased as follows:

"Estimate the state vector $X(t_\ell)$ from the set $\{\theta_m(t_k),\ k \in I\} \cup \{\theta_{D,m}(t_k),\ k \in D\}$". Note that $\{\theta_m(t_k),\ k \in I\} \cap \{\theta_{D,m}(t_k),\ k \in D\}$ is not necessarily empty.

In the following section, we present the computation of the CRLB.

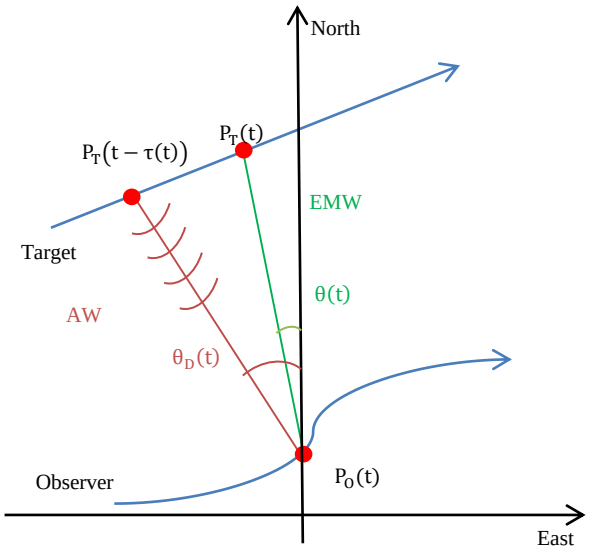


Fig. 1. Example of scenario

III. Asymptotic Performances

The Cramér-Rao Lower Bound being the inverse of the Fisher information matrix (FIM), we develop the computation of the FIM for the state vector $X(t_\ell) \triangleq [x_T(t_\ell) \quad y_T(t_\ell) \quad \dot{x}_T \quad \dot{y}_T]^T$ (also denoted X_ℓ subsequently) for $\ell = 1, 2, \dots$ given by the well-known formula:

$$F(X_\ell) = \sum_{k \in I} \frac{1}{\sigma^2} \nabla_{X_\ell}\theta(X_\ell, t_k)\, \nabla^T_{X_\ell}\theta(X_\ell, t_k) + \sum_{k \in D} \frac{1}{\sigma_D^2} \nabla_{X_\ell}\theta_D(X_\ell, t_k)\, \nabla^T_{X_\ell}\theta_D(X_\ell, t_k)$$

Since

$$X_k = \Phi_{k,\ell}.X_\ell \tag{1}$$

with

$$\Phi_{k,\ell} = \begin{bmatrix} 1 & 0 & t_k - t_\ell & 0 \\ 0 & 1 & 0 & t_k - t_\ell \\ 0 & 0 & 1 & 0 \\ 0 & 0 & 0 & 1 \end{bmatrix},$$

the computation of $\nabla_{X_\ell}\theta(X_\ell, t_k)$ and $\nabla_{X_\ell}\theta_D(X_\ell, t_k)$ can be easily performed by

$$\nabla_{X_\ell}\theta(X_\ell, t_k) = \nabla_{X_\ell}X_k \nabla_{X_k}\theta(X_k, t_k) = \Phi^T_{k,\ell}\nabla_{X_k}\theta(X_k, t_k)$$

and

$$\nabla_{X_\ell}\theta_D(X_\ell, t_k) = \nabla_{X_\ell}X_k \nabla_{X_k}\theta_D(X_k, t_k) = \Phi^T_{k,\ell}\nabla_{X_k}\theta_D(X_k, t_k),$$

where $\nabla_{X_k}\theta(X_k, t_k)$ and $\nabla_{X_k}\theta_D(X_k, t_k)$ are detailed hereafter.

From [3], we have

$$\nabla_{X_k}\theta(X_k, t_k) = \frac{1}{r(t_k)}[\cos\theta(t_k) \quad -\sin\theta(t_k) \quad 0 \quad 0]^T$$

and the components of $\nabla_{X_k}\theta_D(X_k, t_k)$ are

$$\frac{\partial\theta_D(t_k)}{\partial x_T(t_k)} = \frac{1}{\left\|P_T(t_k - \tau(t_k)) - P_O(t_k)\right\|}\{\cos\theta_D(t_k) + \sin\theta_D(t_k)\left[\frac{\dot y_T \sin\theta_D(t_k) - \dot x_T \cos\theta_D(t_k)}{c + \dot x_T \sin\theta_D(t_k) + \dot y_T \cos\theta_D(t_k)}\right] \tag{2}$$

$$\frac{\partial\theta_D(t_k)}{\partial y_T(t_k)} = \frac{1}{\left\|P_T(t_k - \tau(t_k)) - P_O(t_k)\right\|}\{-\sin\theta_D(t_k) + \cos\theta_D(t_k)\left[\frac{\dot y_T \sin\theta_D(t_k) - \dot x_T \cos\theta_D(t_k)}{c + \dot x_T \sin\theta_D(t_k) + \dot y_T \cos\theta_D(t_k)}\right] \tag{3}$$

$$\frac{\partial\theta_D(t_k)}{\partial \dot x_T} = -\tau(t_k)\frac{\partial\theta_D(t_k)}{\partial x_T(t_k)} \tag{4}$$

$$\frac{\partial\theta_D(t_k)}{\partial \dot y_T} = -\tau(t_k)\frac{\partial\theta_D(t_k)}{\partial y_T(t_k)}. \tag{5}$$

Finally, we get

$$\nabla_{X_\ell}\theta(X_\ell, t_k) = \frac{1}{r(t_k)}\begin{bmatrix} \cos\theta(t_k) \\ -\sin\theta(t_k) \\ (t_k - t_\ell)\cos\theta(t_k) \\ -(t_k - t_\ell)\sin\theta(t_k) \end{bmatrix} \tag{6}$$

and

$$\nabla_{X_\ell}\theta_D(X_\ell, t_k) = \begin{bmatrix} \frac{\partial\theta_D(t_k)}{\partial x_T(t_k)} \\ \frac{\partial\theta_D(t_k)}{\partial y_T(t_k)} \\ \left(t_k - t_\ell - \tau(t_k)\right)\frac{\partial\theta_D(t_k)}{\partial x_T(t_k)} \\ \left(t_k - t_\ell - \tau(t_k)\right)\frac{\partial\theta_D(t_k)}{\partial y_T(t_k)} \end{bmatrix} \tag{7}$$

Note that for $\ell = 1$, we find the result given in [15].

IV. ESTIMATION

We propose two estimates of the target's trajectory. First the maximum likelihood estimator of X_ℓ, which is computed in a batch routine, and then a recursive estimator based on the extended Kalman filter (EKF). With the EKF, we estimate recursively X_k at each new measurement.

A. *Batch estimator: Maximum Likelihood Estimator (MLE)*

The maximum likelihood estimator (MLE), which is identical to the least squares estimator since the noises are assumed to be Gaussian, minimizes the following criterion

$$C(X_\ell) = \sum_{k \in I} \frac{1}{\sigma^2}[\theta_m(t_k) - \theta(X_\ell, t_k)]^2 + \sum_{k \in D} \frac{1}{\sigma_D^2}\left[\theta_{D,m}(t_k) - \theta_D(X_\ell, t_k)\right]^2$$

The Gauss-Newton (GN) routine is employed for this minimization. The Hessian is nothing else but $F(X_\ell)$ during iterations. This estimator was presented in [15].

B. *Recursive estimator: Extended Kalman Filter estimator (EKF)*

We develop hereafter the equations of the EKF for the state equation, deduce from (1),

$$X_k = \Phi_{k,k-1}X_{k-1}$$

coupled with a measurement equation which, depending on time t_k is 1 or 2-dimensional:

$$Y_k = \theta_m(t_k) = \theta(X_k, t_k) + \varepsilon(t_k), \qquad \text{if } k \in I \text{ only,}$$

or

$$Y_k = \theta_{D,m}(t_k) = \theta_D(X_k, t_k) + \varepsilon_D(t_k), \qquad \text{if } k \in D \text{ only,}$$

or

$$Y_k = \begin{bmatrix} \theta(X_k, t_k) \\ \theta_D(X_k, t_k) \end{bmatrix} + \begin{bmatrix} \varepsilon(t_k) \\ \varepsilon_D(t_k) \end{bmatrix}, \qquad \text{if } k \in I \cap D.$$

Thus, whatever the case, the k-th measurement can be written as

$$Y(t_k) = \mathcal{H}_k\big(X(t_k)\big) + e_k\,,$$

$$\text{with } e_k = \varepsilon(t_k) \text{ or } \varepsilon_D(t_k) \text{ or } \begin{bmatrix} \varepsilon(t_k) \\ \varepsilon_D(t_k) \end{bmatrix}$$

In short, the state system is composed of a linear state equation and a nonlinear measurement equation whose dimension can change along the scenario. The EKF algorithm is given by the following equations:

$$X_{k/k-1} = F_k . X_{k-1/k-1}$$

$$P_{k/k-1} = F_k . P_{k-1/k-1} . F_k^T$$

$$K_k = P_{k/k-1} . H_k^T \big[H_k . P_{k/k-1} . H_k^T + R_k\big]^{-1}$$

$$X_{k/k} = X_{k/k-1} + K_k \left(Y_k - \mathcal{H}_k\big(X_{k/k-1}\big)\right)$$

$$P_{k/k} = (I_4 - K_k . H_k) . P_{k/k-1} . (I_4 - K_k . H_k)^T + K_k R_k K_k^T$$

where H_k is the Jacobian of $\mathcal{H}_k(.)$ at $X_{k/k-1}$:

$$H_k = \nabla_{X_k}^T \mathcal{H}_k\big(X_{k/k-1}\big) = \begin{cases} \nabla_{X_k}^T \theta(X_k, t_k)_{|X_k = X_{k/k-1}} & \text{if } k \in I \text{ only,} \\ \nabla_{X_k}^T \theta_D(X_k, t_k)_{|X_k = X_{k/k-1}} & \text{if } k \in D \text{ only,} \\ \begin{bmatrix} \nabla_{X_k}^T \theta(X_k, t_k) \\ \nabla_{X_k}^T \theta_D(X_k, t_k) \end{bmatrix}_{|X_k = X_{k/k-1}} & \text{if } k \in I \cap D. \end{cases}$$

where the gradients are given by (6) and (7), with ℓ=k.

V. Numerical Application

This section focuses on the study of the empirical performances of the MLE and EKF estimators on different scenarios. The following results are obtained with 500 Monte-Carlo simulations.

The GN routine is initialized with $X_{init} = r_{init}\big[\sin\big(\theta_m(t_1)\big) \quad \cos\big(\theta_m(t_1)\big) \quad 0 \quad 0\big]$.

And the EKF is initialized as follows:

$$X_{0/0} = X_{init} \text{ and } P_{0/0} = \begin{bmatrix} \frac{20000^2}{12} & & & \\ & \frac{20000^2}{12} & & 0 \\ & & \frac{10}{12} & \\ & 0 & & \frac{10}{12} \end{bmatrix}$$

where the initialized range r_{init} is arbitrary chosen.

Hereafter, the MLE and the EKF algorithm are performed on 6 different scenarios. Two types of scenarios are used in our study: long range scenarios, and short range scenarios. In long range scenarios, passive radar and passive sonar are mounted on the platform. The respective sampling periods of radar and sonar are $\Delta t = 1$s. and $\Delta t_D = 4$s. The respective standard deviations of the instantaneous bearings and delayed bearings are $\sigma = 1°$ and $\sigma_D = 1°$. In short range scenarios, passive radar is replaced by a periscope with $\Delta t = 120$s, and $\sigma = 0.1°$. The sound propagation speed is chosen to be equal to 1500m/s. The observer changes its heading. Note that in all these scenarios, the initial position of the observer is $P_O(0) = [0 \quad 0]^T$.

The performances of the estimated state vector at final time obtained with the MLE and the EKF algorithm, as well, are given in tables. We compute the empirical biases and standard deviations of each estimator (denoted $\hat{\sigma}_{MLE}$ and $\hat{\sigma}_{EKF}$) and the asymptotic performance given by the square root of the diagonal element of the CRLB (denoted σ_{CRLB}). Moreover, to quantify the interest of ITTMA, the asymptotic performance of the classical BOTMA (denoted σ_{CRLB}^{BOTMA}) are given in tables. For each scenario, four figures are plotted. Fig. (a) depicts the observer's and the target's trajectory. The letters "O" and "T" designate their respective initial positions; the 90% confidence ellipsoids from the CRLB are centered on the true target's location at three different instants and the 500 MLE estimated positions at the same instants. On Fig (b), the 500 EKF outputs are plotted. Fig. (c) and Fig. (d) are the respective magnifications of Fig. (a) and Fig (b), around the end of the scenario.

A. *Scenario 1: Long range (passive sonar and passive radar)*

The duration of scenario 1 is 20 minutes (1200 seconds). During the first 200 seconds, the observer is in CV motion with a speed equal to 7m/s and a heading of 90°, then during 400 seconds, it is in constant turn (CT) with a turn rate of $-20°$/min, and for the last 600 seconds it is anew in CV motion with a speed equal to 7m/s and a heading of $-45°$. The initial position of the target is $P_T(0) = [15 \quad 18]^T$(km); its speed is equal to 5 m/s and its heading is 150°. For the initialization, we chose $r_{init} = 10$ km.

Fig. 2 depicts the 90% confidence ellipses at 400s, 800s, and 1200s, and the 500 estimated positions at the same instants. After the first 7 minutes, the cloud to the 500 MLE is within the confidence ellipses, unlike the EKF which appears biased. The correct performance of the MLE is maintained up to the end of the scenario. The EKF has to wait 13 minutes to behave properly, even though the computed estimators are not strictly efficient. Table I corroborates this fact.

B. *Scenario 2: Short range (passive sonar and periscope)*

Now, the duration of the scenario is 10 minutes (600s). During the first 100 seconds, the observer is in CV motion with a speed equal to 7m/s and a heading of 90°, then during 400 seconds it is in CT with a turn rate of $-20°$/min, and for the last 100 seconds it returned in CV motion with a speed equal to 7m/s and a heading of $-45°$. The target starts from

$P_T(0) = [4 \quad 6]^T$ (km) with a speed equal to 5 m/s and a heading of 150°. For this scenario, we chose $r_{init} = 10$ km.

Fig. 3 depicts the 90% confidence ellipses at 200s, 400s and 600s and the 500 estimated positions at the same instants. Again, the MLE behaves accordingly to the theory for this scenario, where its efficiency is confirmed (see Table II). The EKF does not diverge (the cloud of estimates remains in a "reasonable" zone), but it is not efficient. Note that σ_{CRLB}^{BOTMA} is three times bigger than σ_{CRLB}. This improvement is due to the 5 instantaneous bearing measurements only.

C. Scenario 3: Long range (passive sonar and a passive radar)

The trajectory of the observer is the same as in scenario 1. The target's initial position is $P_T(0) = [15 \quad 18]^T$ (km); its speed is equal to 5 m/s and its heading is $-90°$. We choose $r_{init} = 30$ km.

As shown in Fig. 4, the MLE is practically unbiased (see Table III). The EKF is biased but its outputs are in the vicinity of the target's trajectory.

D. Scenario 4: Short range (passive sonar and periscope)

The duration of the scenario and the observer's trajectory are the same as scenario 2. Only the target's trajectory changed. The target starts from $P_T(0) = [4 \quad 6]^T$ (km) with a speed equal to 5 m/s and a heading of $-90°$. The GN routine and the EKF were initialized with $r_{init} = 10$ km.

Fig. 5 depicts the 90% confidence ellipses at 200s, 400s, and 600s, and the 500 estimated positions at the same instants. The EKF performs poorly whereas the MLE is quasi unbiased and its covariance matrix (not reported here) is very close to the CRLB.

E. Scenario 5: Long range (passive sonar and a passive radar)

This scenario is an extension of scenario 1; now its duration is 30 minutes, and the observer makes a second change of heading: 20 minutes after the beginning, the observer starts its maneuver by a CT during 6min 40s with a turn rate of 20°/min, then it finishes its route in a CV motion during 3min 20s, and an heading of 90°.

Fig. 6 shows the 90% confidence ellipsoids at 600s, 1200s, and 1800s, and the 500 estimated positions at the same instants. The MLE keeps its excellent performance, and the EKF, even if it is not efficient in a strict sense, behaves properly (see Table V).

F. Scenario 6: Short range (passive sonar and periscope)

This scenario is the prolongation of scenario 2: the target keeps its route, but the observer makes a second turn after 10 mn: it starts a CT motion with turn rate of 20°/min, and after 6min 40s, it returns in CV motion during 3min 20s. The total duration of scenario 6 is hence 20 minutes.

The 500 estimated positions and the 90% confidence ellipses at 400s, 800s, and 1200s are depicted in Fig. 7.

Fig. 7 shows that the EKF does not benefit from the additional maneuver, conversely to the MLE which keeps its efficiency. Table VI corroborates this assertion.

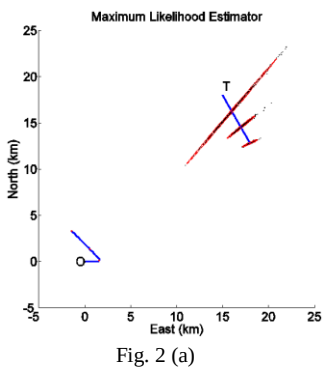


Fig. 2 (a)

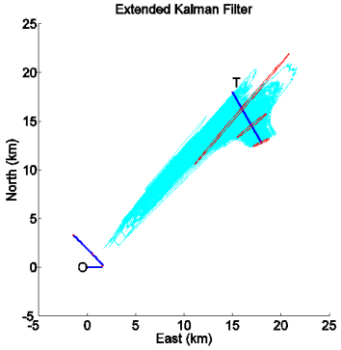


Fig. 2 (b)

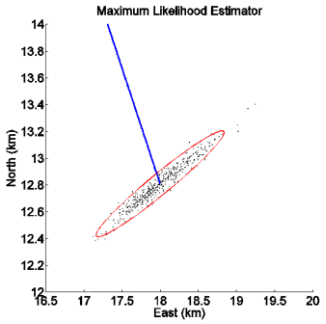


Fig. 2 (c)

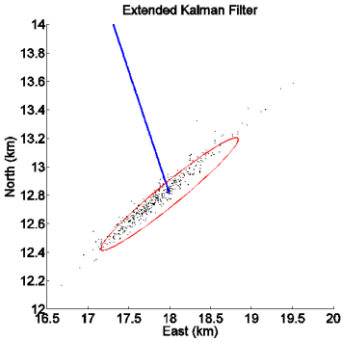


Fig. 2 (d)

Fig. 2. Scenario 1: observer's and target's trajectories, the three 90% confidence ellipse, the estimated positions.

TABLE I. PERFORMANCES OF THE MLE AND EKF ESTIMATORS IN SCENARIO 1.

X_M	Bias MLE	Bias EKF	$\hat{\sigma}_{MLE}$	$\hat{\sigma}_{EKF}$	σ_{CRLB}	σ_{CRLB}^{BOTMA}
$x_T =$ 17998 (m)	0.1923	191.26	337.66	415.71	342.38	770.37
$y_T =$ 12808 (m)	0.9215	46.34	158.84	202.28	161.52	367.51
$\dot{x}_T = 2.5$ (m/s)	0.0030	0.4719	0.3059	0.2891	0.2985	0.6717
$\dot{y}_T =$ −4.33 (m/s)	0.0052	0.7283	0.5510	0.5049	0.5463	1.2383

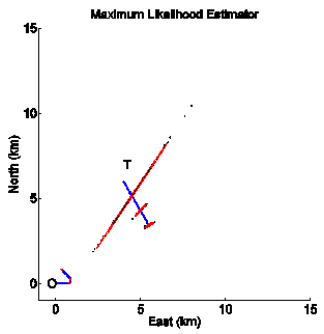


Fig. 3 (a)

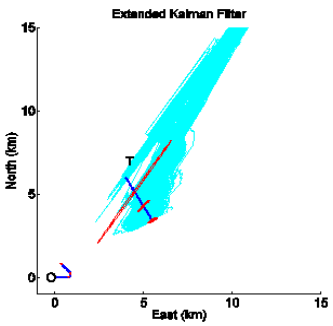


Fig. 3 (b)

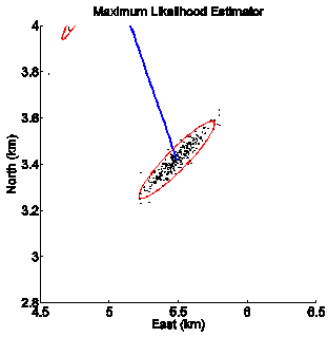


Fig. 3 (c)

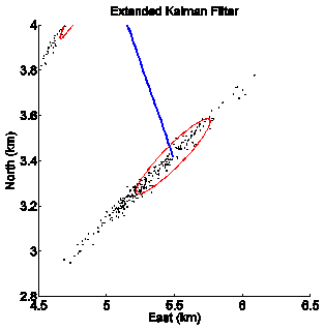


Fig. 3 (d)

Fig. 3. Scenario 2: observer's and target's trajectories, the three 90% confidence ellipses, the estimated positions.

TABLE II. PERFORMANCES OF THE MLE AND EKF ESTIMATORS IN SCENARIO 2.

X_M	Bias MLE	Bias EKF	$\hat{\sigma}_{MLE}$	$\hat{\sigma}_{EKF}$	σ_{CRLB}	σ_{CRLB}^{BOTMA}
x_T = 5490 (m)	0.8812	178.44	110.78	259.79	111.61	356.99
y_T = 3419 (m)	1.8935	101.44	67.13	154.14	68.00	189.94
$\dot{x}_T = 2.5$ (m/s)	0.0027	0.5285	0.2279	0.1839	0.2208	0.4319
$\dot{y}_T = -4.33$ (m/s)	0.0070	0.0877	0.4804	0.5683	0.4670	1.2481

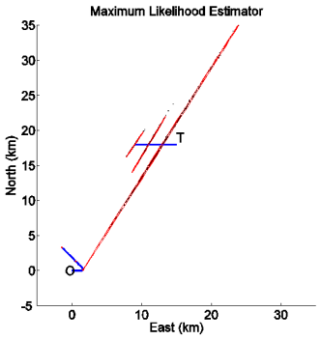


Fig. 4 (a)

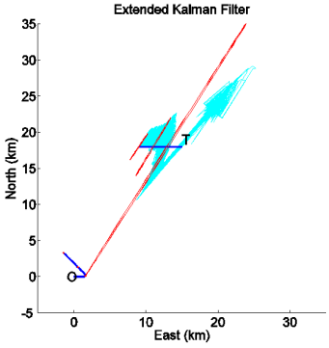


Fig. 4 (b)

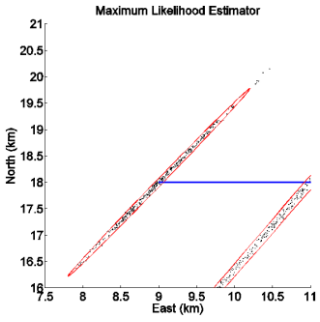


Fig. 4 (c)

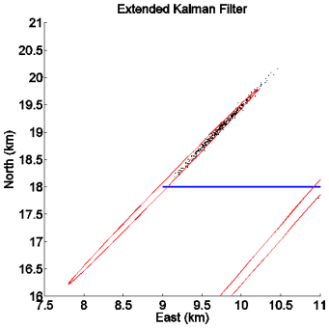


Fig. 4 (d)

Fig. 4. Scenario 3: observer's and target's trajectories, the three 90% confidence ellipses, the estimated positions.

TABLE III. PERFORMANCES OF THE MLE AND EKF ESTIMATORS IN SCENARIO 3.

X_M	Bias MLE	Bias EKF	$\hat{\sigma}_{MLE}$	$\hat{\sigma}_{EKF}$	σ_{CRLB}	σ_{CRLB}^{BOTMA}
x_T = 9005 (m)	6.82	735.98	492.39	251.91	489.70	1102.04
y_T = 18000 (m)	11.75	1082.3	728.35	381.70	725.39	1623.42
$\dot{x}_T = -5$ (m/s)	0.0013	0.7742	0.6132	0.2334	0.6045	1.3613
$\dot{y}_T = 0$ (m/s)	0.0058	1.0990	0.8789	0.3358	0.8672	1.9418

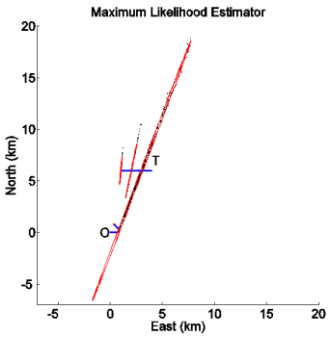


Fig. 5 (a)

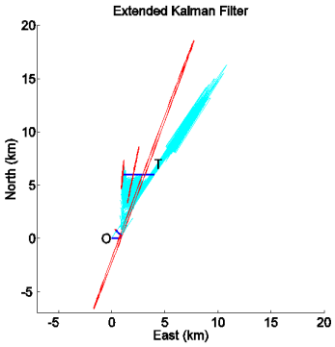


Fig. 5 (b)

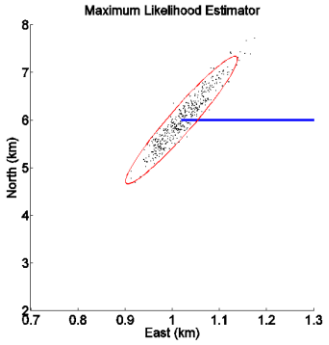


Fig. 5 (c)

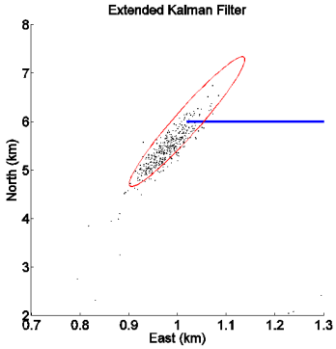


Fig. 5 (d)

Fig. 5. Scenario 4: observer's and target's trajectories, the three 90% confidence ellipses, the estimated positions.

TABLE IV. PERFORMANCES OF THE MLE AND EKF ESTIMATORS IN SCENARIO 4.

X_M	Bias MLE	Bias EKF	$\hat{\sigma}_{MLE}$	$\hat{\sigma}_{EKF}$	σ_{CRLB}	σ_{CRLB}^{BOTMA}
x_T = 1020 (m)	5.22	46.10	49.22	68.56	48.42	96.73
y_T = 6000 (m)	66.81	627.98	558.04	647.13	546.55	897.54
$\dot{x}_T = -5$ (m/s)	0.0280	0.2967	0.2360	0.2668	0.2297	0.3189
$\dot{y}_T = 0$ (m/s)	0.0584	0.3725	0.5002	0.6650	0.4923	0.9184

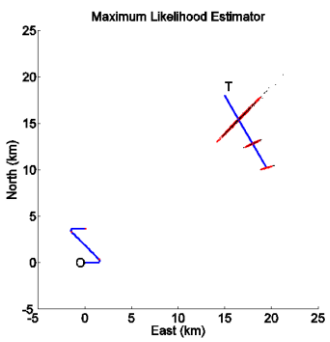


Fig. 6 (a)

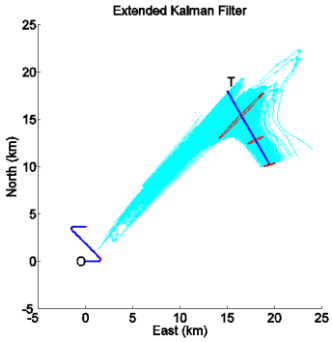


Fig. 6 (b)

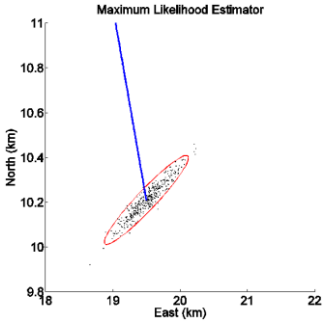


Fig. 6 (c)

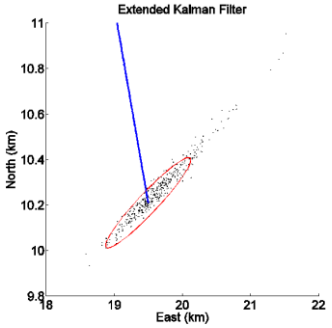


Fig. 6 (d)

Fig. 6. Scenario 5: observer's and target's trajectories, the three 90% confidence ellipses, the estimated positions.

TABLE V. PERFORMANCES OF THE MLE AND EKF ESTIMATORS IN SCENARIO 5.

X_M	Bias MLE	Bias EKF	$\hat{\sigma}_{MLE}$	$\hat{\sigma}_{EKF}$	σ_{CRLB}	σ_{CRLB}^{BOTMA}
$x_T = 19498$ (m)	1.92	152.40	252.66	413.99	255.10	570.02
$y_T = 10210$ (m)	2.67	59.92	79.28	146.24	81.01	183.17
$\dot{x}_T = 2.5$ (m/s)	0.0046	0.1035	0.0931	0.2756	0.0967	0.2159
$\dot{y}_T = -4.33$ (m/s)	0.0057	0.0402	0.0995	0.3317	0.1007	0.2262

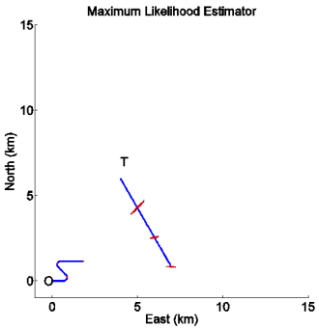


Fig. 7 (a)

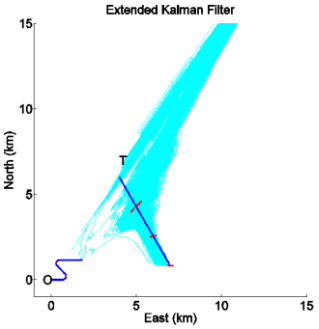


Fig. 7 (b)

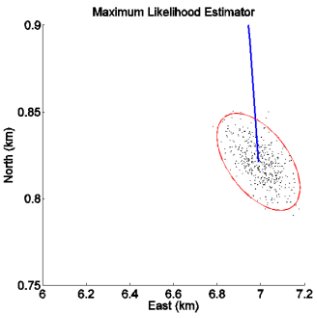


Fig. 7 (c)

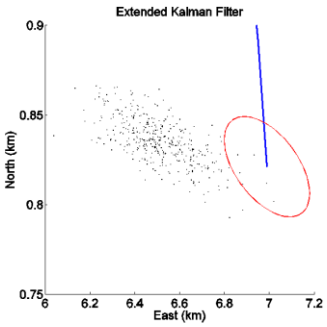


Fig. 7 (d)

Fig. 7. Scenario 6: observer's and target's trajectories, the three 90% confidence ellipses, the estimated positions.

TABLE VI. PERFORMANCES OF THE MLE AND EKF ESTIMATORS IN SCENARIO 6.

X_M	Bias MLE	Bias EKF	$\hat{\sigma}_{MLE}$	$\hat{\sigma}_{EKF}$	σ_{CRLB}	σ_{CRLB}^{BOTMA}
$x_T = 6990$ (m)	7.12	484.98	77.07	215.53	77.78	201.03
$y_T = 821$ (m)	0.18	14.91	11.43	19.73	11.41	21.45
$\dot{x}_T = 2.5$ (m/s)	0.0041	0.3974	0.0391	0.1112	0.0400	0.1044
$\dot{y}_T = -4.33$ (m/s)	0.0052	0.2464	0.0702	0.1883	0.0695	0.1649

VI. CONCLUSION

In FUSION'15, we proposed a novel TMA, called inverse triangulation TMA, by exploiting the angles of electromagnetic wave's arrival and of acoustic wave's arrival. The key of inverse triangulation TMA is to take the propagation delay of the acoustic waves into account. This paper is the extension of this study: we considered a maneuvering platform and used the maximum likelihood estimator together with the extended Kalman filter, both in Cartesian coordinates. The MLE is definitively efficient for this problem. The Cartesian EKF returns estimators which are in the vicinity of the true state vector. However, strictly speaking, it is not efficient, and takes no benefit of a second observer's maneuver. More subtly, its behavior depends on the sampling period of the so-called instantaneous bearings: it seems to be insensitive to these additional measurements when the sampling period is about 2 minutes, even with very accurate bearings. The research effort must hence be focused upon the EKF, for instance in changing the coordinates systems (for example we could try the modified polar coordinates), or in changing the equation of the EKF by extending its linearization in second order. Another point merits to be studied: in real situations, the acoustic bearings can be biased due to propagation phenomena. This bias has to be taken into account. This is still under investigation.

REFERENCES

[1] V.J. Aidala, "Kalman Filter Behavior in Bearings-Only Tracking Applications", *IEEE Transaction on Aerospace and Electronic Systems*, AES-15, no. 1, pp. 29-39, January 1979.

[2] A.G. Lindgren, K.F. Gong, "Position and Velocity Estimation via Bearing Observations", *IEEE Transaction on Aerospace and Electronic Systems*, AES-14, no. 4, pp. 564-577, July 1978.

[3] S.C. Nardone, A.G. Lindgren, and K.F. Gong, "Fundamental Properties and Performance of Conventional Bearings Only Target Motion Analysis" *IEEE Transactions on Automatic Control*, AC-29, 9, pp. 775-787, September 1984.

[4] V.J. Aidala and S. Hammel, "Utilization of Modified Polar Coordinates for Bearings-Only Tracking" *IEEE Transactions on Automatic Control*, AC-28, 3, pp. 283-294, March 1983.

[5] J.P. Le Cadre, C. Jauffret, "Discret-Time Observability and Estimability Analysis for Bearings-Only Target Motion Analysis", *IEEE Transaction on Aerospace and Electronic Systems*, AES-33, no. 1, pp. 178-201, January 1997.

[6] S.C. Nardone, V.J. Aidala, "Observability Criteria for Bearings-Only Target Motion Analysis", *IEEE Transaction on Aerospace and Electronic Systems*, AES-17, no. 2, pp. 162-166, March 1981.

[7] C. Jauffret, D. Pillon, "Observability in Passive Target Motion Analysis", *IEEE Transaction on Aerospace and Electronic Systems*, AES-32, no. 4, pp. 1290-1300, October 1996.

[8] C. Jauffret, Y. Bar-Shalom, "Track Formation with Bearing and Frequency Measurements in Clutter", *IEEE Transaction on Aerospace and Electronic Systems*, AES-26, no. 6, pp. 999-1009, November 1990.

[9] J.M. Passerieux, D. Pillon, P. Blanc-Benon, C. Jauffret, "Target Motion Analysis with Bearing and Frequencies Measurements", *Proceeding of the 22nd Asilomar Conference*, Pacific Grove, CA, USA, November 1988.

[10] C. Jauffret, P. Blanc-Benon, D. Pillon, "Multi Frequencies And Bearing Target Motion Analysis : Properties and Sonar Applications", *Proceeding of the 11th International Conference on Information Fusion (FUSION 2008)*, Cologne, Germany, July 2008.

[11] C. Jauffret, D. Pillon, A.C. Pignol, "Leg-by-leg Bearings-Only TMA without Observer Maneuver", in *Journal of Advanced Information Fusion*, Vol. 6, no. 1, pp. 24-38, June 2011.

[12] J. Clavard, D. Pillon, A.C. Pignol, C. Jauffret, "Target Motion Analysis of a Source in Constant Turn from a Nonmaneuvring Observer", *IEEE Transaction on Aerospace and Electronic Systems*, AES-49, no. 3, pp. 1760-1780, July 2013.

[13] C. Jauffret, D. Pillon, A.C. Pignol, "Bearings-Only Maneuvring Target Motion Analysis from a Nonmaneuvring Platform", *IEEE Transaction on Aerospace and Electronic Systems*, AES-46, no. 4, pp. 1934-1948, October 2010.

[14] R. Yang, G.W. Ng, Y. Bar-Shalom, "Bearings-Only Tracking with Fusion from Heterogenous Passive Sensors: ESM/EO and Acoustic", *Proceeding of 18th International Conference on Information Fusion (FUSION 2015)*, Washington D.C., USA, July 2015.

[15] C. Jauffret, A.C. Pérez-Pignol, "Target Motion Analysis by Inverse Triangulation", *Proceeding of 18th International Conference on Information Fusion (FUSION 2015)*, Washington, D.C., USA, July 2015.

[16] K.W. Lo, B.G. Ferguson, "Broadband Passive Acoustic Technique for Target Motion Analysis Parameter Estimation", *IEEE Transaction on Aerospace and Electronic Systems*, AES-36, no. 1, pp. 163-175, January 2000.

[17] U. Orguner, F. Gustafsson, "Target Tracking Using Delayed Measurements with Implicit Constaints", *Proceeding of 11th International Conference on Information Fusion (FUSION 2008)*, Cologne, Germany, July 2008.

[18] U. Orguner, F. Gustafsson, "Disturbed Target Tracking with Propagation Delayed Measurements", *Proceeding of 12th International Conference on Information Fusion (FUSION 2009)*, Seattle, USA, July 2009.

[19] U. Orguner, F. Gustafsson, "Target Tracking with Particle Filters Under Signal Propagation Delays", *IEEE Transaction on Signal Processing*, 59, 6, pp. 2485-2495, June 2011.

[20] S.Z. Bi, X.Y. Ren, "Maneuvring Target Doppler-Bearing Tracking Using Interacting Multiple Models Algorithm", *Progress In Electromagnetics Research (PIER 87)*, pp. 15-41, 2008.

[21] Y. Guo, A. Xue, D. Peng, "A Recursive Algorithm for Bearings-Only Tracking with Signal Time Delay", *Signal Processing*, 88, 6, pp. 1539-1552, 2008.

[22] B. Cheung, S. Davy, D. Gray, "PMHT for Tracking with Timing Uncertainty", *Proceeding of 13th International Conference on Information Fusion (FUSION 2010)*, Edinburg, Scotland, July 2010.

[23] R. Yang, Y. Bar-Shalom, J.H. Huang, G.W. Ng, "Interacting Multiple Model Unscented Gauss-Helmert Filter for Bearings-Only Tracking with State-Dependent Propagation Delay", *Proceeding of 17th International Conference on Information Fusion (FUSION 2014)*, Salamanca, Spain, July 2014.